Journal of Materials Chemistry A

PAPER

View Article Online
View Journal | View Issue

Cite this: J. Mater. Chem. A, 2015, 3, 9638

Incorporation of Ag nanowires in $CuWO_4$ for improved visible light-induced photoanode performance

H. Zhang, P. Yilmaz, J. O. Ansari, F. F. Khan, R. Binions, S. Krause and S. Dunn*

We report the sol–gel synthesis of a $CuWO_4$ ($E_g \sim 2.0$–2.15 eV) thin film loaded with Ag nanowires. The incorporation of Ag nanowires into the semiconductor matrix significantly improves the performance of $CuWO_4$ as a photoanode for use in photochemical water splitting (PEC). Here, we have developed a planar electrode to test the photoactivity of the catalyst using standard electrochemical procedures under simulated solar light. The sol–gel synthesis of $CuWO_4$ is modified such that we add Ag nanowires during sol aging. We demonstrate that there is negligible change to the $CuWO_4$ matrix microstructure, morphology or crystal structure. When we compare the pristine $CuWO_4$ to the material with Ag nanowires embedded in the $CuWO_4$ matrix there is a fourfold improvement of photocurrent at 1.23 V *vs.* NHE to *ca.* 1.5 mA cm^{-2} (pH 9) under simulated AM1.5G illumination. This photocurrent is very competitive against more well developed photoanode structures when consideration for surface area is allowed. The Ag nanowires increase carrier mobility film enabling a sufficiently thick sample of catalyst, measured at 750 nm, to effectively harvest incident light. The addition of the Ag nanowires removes the plateau region found for $CuWO_4$ further indicating that there is a good flow of carriers to the surface of the catalyst, a significant improvement as carrier mobility has been shown to be low in $CuWO_4$. The Faradaic efficiency of the catalyst was measured at 31%. Our flat band potential is found to be 0 *vs.* NHE. The ability to make a highly photoactive catalyst using a simple chemical process opens up opportunities in a wide range of areas that focus on PEC and other light harvesting processes.

Received 31st December 2014
Accepted 26th March 2015

DOI: 10.1039/c4ta07213h

www.rsc.org/MaterialsA

Introduction

Since discovering a photocatalyst could oxidise water and produce a solar fuel[1] there has been interest in developing systems for the production of solar fuels.[2–4] TiO_2 shows many desirable properties for the production of a solar fuel, it is stable under illumination and shows good surface activity.[5,6] The selection of catalysts with respect to solubility[7] remains a key issue in semiconductor choice. In addition there are problems associated with carrier recombination and separation of reaction products.[8,9] However the most significant problem with TiO_2 is a band gap of *ca.* 3.2 eV meaning only 3–4% of solar light can generate photoexcited carriers. This limitation has driven an on-going search for active and stable narrow band gap catalysts. A range of techniques have been applied to solving the problem of light harvesting for TiO_2.[10] However, a significant problem is that narrow band gap materials are prone to photodegradation when illuminated.

The current list of interesting materials include Fe_2O_3,[11,12] WO_3,[13,14] $BiVO_4$ (ref. 15 and 16) and $CuWO_4$ (ref. 17 and 18) as well as polar materials such as $BaTiO_3$,[2,4,19] $PbZr_xTi_{1-x}O_3$ (ref. 9 and 20–23) and $LiNbO_3$.[24–26] These materials show a range of interesting properties but have some negative aspects. For example problems exist with grain boundary recombination and short diffusion lengths in Fe_2O_3.[27] WO_3 has been extensively studied due to the visible band gap around 2.7 eV.[28,29] Darwent and Mills[13] showed WO_3 could oxidise water while adding RuO_2 significantly increased reaction rate. The low overpotential for oxygen liberation over RuO_2 was the given explanation associated with good light harvesting. However, a disadvantage of WO_3 is the poor stability in neutral or basic aqueous solutions.

A material that has the potential to mitigate problems with stability is $CuWO_4$. The material has been shown to be stable in a photochemical cell under illumination and has a very well positioned valence band for water oxidation and a band gap of 2.3 eV indicates that the material is also visible active. Bartlett[17] described the narrowing of the band gap due to the lifting of the valence band maximum with an interaction of Cu(3d) and O(2p) orbitals, and provides some detail on band structure and light harvesting. Coupling $CuWO_4$ with WO_3 produced a catalyst that appeared to be stable and showed zero bias formation of O_2 using ferric cyanide as a mediator. $CuWO_4$ has been identified as a gas sensor[30] so a number of methods for synthesis have been identified.[31]

Materials Research Institute, School of Engineering and Materials Science, Queen Mary University of London, Mile End Road, London E1 4NS, UK. E-mail: s.c.dunn@qmul.ac.uk

$CuWO_4$ is an indirect n-type semiconductor hence a relatively thick layer of material is required for absorption of light, a disadvantage of $CuWO_4$. Further the carrier mobility of $CuWO_4$ is limited due to trap states associated with Cu d orbital electrons. Hence, the production of a layer sufficient to absorb light shows little photocurrent. The low photocurrent is also associated with slow surface kinetics and reduced chemical efficiency. $CuWO_4$ has a flat band potential and carrier density +0.4 V (*vs.* NHE) and 2.7×10^{21} cm^{-3} close to that measured for WO_3. At +0.4 V (*vs.* NHE) the E_{fb} is suitable for water oxidation and $CuWO_4$ is a candidate photoanode material.

Typical strategies to overcome low carrier mobility are to produce nanostructures with dimensions on the order of the diffusion length of carriers. This has been effective for Fe_2O_3 and $BiVO_4$. However, this is not viable for $CuWO_4$ due to the indirect semiconductor properties. Gaillard reported a significant increase in the photocurrent for $CuWO_4$ by adding carbon nanotubes (CNT) into the structure.[32] However, CNT are not photoactive in the structure nor are they photocatalytic.

The CNT's overcome limitations of carrier mobility by providing alternative pathways for carrier migration. CNT's have a range of interesting electronic characteristics but have not shown catalytic performance. The addition of CNT's shows some improvement in current, but the currents are still relatively low which is likely due to slow reaction kinetics at the material surface. An interesting diversion from the current range of research would be incorporating a catalytically active and conductive material into the $CuWO_4$ photocatalyst. The candidate material that we have investigated was Ag in the form of a nanowire.

Experimental

Sigma-Aldrich provided pre-cursor materials at least 3 9's grade. 0.01 mol of copper nitrate trihydrate ($Cu(NO_3)3H_2O$), was dissolved in 12 mL of ethylene glycol at room temperature under constant stirring. Upon complete dissolution of the copper precursor 0.01 mol ammonium metatungstate trihydrate ($(NH_4)6H_2W_{12}O_{40}$ AMT) and 1 mL deionized H_2O was added. The light blue solution was constantly stirred under sonication until the AMT completely dissolved. At this point 0.25 g of Triton-X 100 ($C_{14}H_{22}O(C_2H_4O)_n$) a commonly used surfactant was added and the solution was then heated to 95 °C for 3 hours while being stirred. The final solution was sealed under air and allowed to cool to room temperature before aging for 2 days.

The substrate used was fluorine doped tin oxide coated float glass (FTO, Tec 15 Pilkington). A 5 cm^2 square of the FTO glass was cut and cleaned by sonication with acetone and ethanol for 20 min before rinsing with deionized water and dried with nitrogen. The substrate was placed on a spin coater and 0.5 mL aged solution dropped onto the centre. Spin speed was ramped from 0 to 500 rpm at 100 rpm s^{-1} and held at 500 rpm for 5 s followed by a 100 rpm s^{-1} ramp to 2000 rpm where it was held for 5 min. The coated substrate was placed on a hot plate at 95 °C for 5 min followed by heating at 300 °C in a pre-heated furnace for 10 min. The sample was then allowed to cool in air before annealing in air 500 °C for 2 hours with a ramp rate of 5 °C min^{-1}. For samples with multiple layers, new layers were added after the 300 °C stage with a final anneal at 550 °C.

Where the sol–gel was modified with Ag nanowires (supplied directly by Sigma Aldrich as part product number 739421, 0.5 wt% in IPA suspension); Ag nanowires were added after one day of sol ageing. This was then subjected to a further day of ageing. Appropriate volumes (0.025–0.1 mL) of Ag nanowire suspension were added into the pre-cursor stock solution. This mixed solution was then sonicated to produce a solution that had no visible changes to the pre-silver solution.

X-ray diffraction (XRD) patterns were obtained with a Panalytical Xpert Pro diffractometer using Cu-Kα radiation. High-resolution scans were obtained in a continuous scan mode at a scan speed of 0.6° min^{-1} with a collection width of 0.0167°. The morphology was observed using a scanning electron microscope (SEM, FEI Inspect F). X-ray photoelectron spectroscopy was carried out at NEXUS using a Kratos Analytical AXIS Nova system, peaks were calibrated to an adventitious C1s peak at 284.1 eV.

Optical absorption was measured using a Perkin Elmer Lambda 950 UV-Vis spectrophotometer. The reference electrode was a saturated Ag/AgCl (supplied by IJ Cambria Scientific) and the counter electrode was Pt mesh. PEC measurements were obtained under AM1.5G simulated solar radiation (Newport solar simulator) and collected using a Gamry Interface 1000 potentiostat at a scan rate of 100 mV s^{-1} in a phosphate buffered saline solution pH 7.4 containing 140 mM NaCl. Mott–Schottky plots were measured using an Autolab PGSTAT 10 with FRA 2 (Windsor Scientific, UK).

Faradaic efficiency was calculated using the optimal volume of gas evolved over the period of reaction against the volume of gas produced from pure water at an applied voltage of 1 V *vs.* SCE. The composition of the gaseous products was determined using gas chromatography (supplied by SRIGC in TCD mode). Where water spitting was tested the electrolyte was water with a resistance greater than 25 MΩ at an applied potential of 1 V after 30 minutes of N_2 purging.

Results and discussion

$CuWO_4$ films with and without Ag nanowires from 200 nm to 900 nm in cross sectional thickness were deposited using spin coating. The structure and morphology of the $CuWO_4$ films was determined using SEM and X-ray diffraction. Fig. 1 shows a typical surface SEM micrograph for $CuWO_4$ exhibiting limited surface topography; the inset shows a cross-section of a 350 nm film with a pseudo globular grain structure around 250 nm in size.

The addition of Ag nanowires did not produce any significant change to microstructure or crystallographic phase of the $CuWO_4$ as shown in Fig. 2. Some minor changes to the diffraction pattern peak intensities were observed and attributed to a change in preferential orientation as a result of a change in the nucleation process as the Ag has been added. This indicates Ag nanowires are being incorporated into the $CuWO_4$ film and only making small alterations to the nucleation mechanisms of the film. As the Ag nanowires are being added to

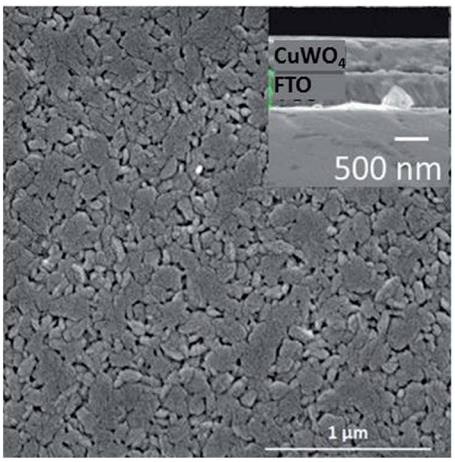

Fig. 1 Typical SEM micrograph of $CuWO_4$ thin film showing limited surface topography, with inset showing a cross section of sample.

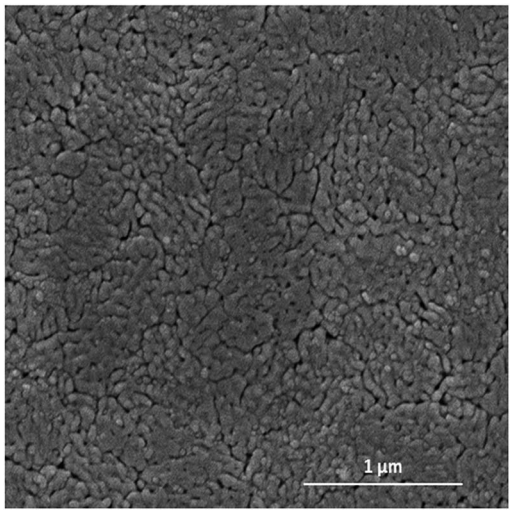

Fig. 2 SEM micrograph of Ag modified $CuWO_4$ showing negligible changes to surface morphology.

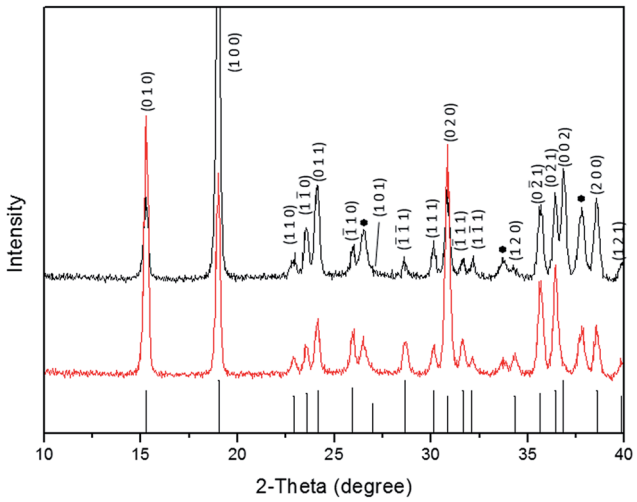

Fig. 3 X-ray diffraction pattern for $CuWO_4$ (top) and $CuWO_4$ (bottom) with the addition of Ag nanowires indicating no substantial change to the crystal structure with the incorporation of Ag.

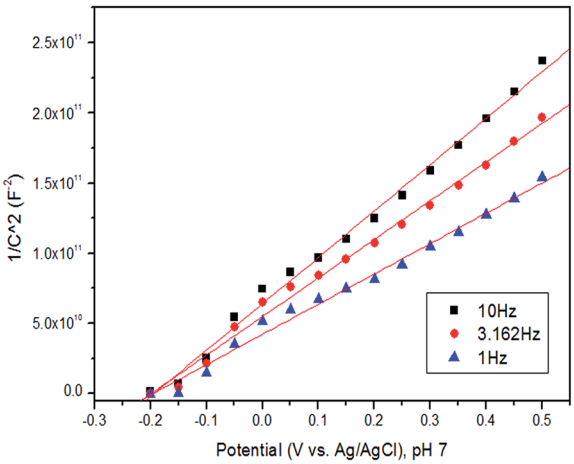

Fig. 4 Mott–Schottky plot for $CuWO_4$ films showing a flat band potential of −0.2 V *vs.* Ag/AgCl (0.0 V *vs.* NHE), the carrier density was calculated to be 5.1×10^{19} cm^{-3}.

the sol during are only small changes to the nucleation process and hence no change in the crystal structure or morphology.

We show an X-ray diffraction pattern associated with two 300 nm thick films of $CuWO_4$, without Ag nanowires and with 0.5% w/w Ag nanowires, Fig. 3. The X-ray diffraction pattern shows a close match to JCPDS 72-0616. Note we do not detect Ag in the XRD pattern or in EDS (performed during SEM analysis) due to the low amount of Ag in the sample; it is below the detection limit for our test systems. In order to determine the chemical state of the Ag we have performed XPS analysis, these results show that Ag is present as we have distinct peaks at 368 eV and 374 eV with the 3d 3/2 and 3d 5/2 peak being separated by 6.05 eV.

A Mott–Schottky plot for pure $CuWO_4$ cross-section 350 nm, Fig. 4, indicates the flat band potential is −0.2 V *vs.* Ag/AgCl (0.0 V *vs.* NHE), and the sample is n-type with a carrier density of 5.1×10^{19} cm^{-3}. This value of the flat band potential (E_{fb}) is also quite consistent with that previously reported for WO_3.[33] The value of E_{fb} we measure is similar to previous reports but the carrier density is two orders of magnitude lower than previous reports.[17] As the Mott–Schottky analysis shows the onset potential for the $CuWO_4$ system is approximately 0 *vs.* NHE indicating that the catalyst is not able to perform the splitting of water in the absence of an external electrical bias.[34]

Our low carrier density is related to the method of synthesis of the material which is annealed under air and results in a small grain structure with a large number of grain boundaries. We, and others, have previously shown that annealing under air and other atmospheres can influence both the concentration of oxygen vacancies[35,36] and the type of other vacancies or defects within a thin film or nanostructured material. Additionally, it is well known that factors such as size of a grain and grain boundaries can influence E_{fb} and carrier mobility of a material

through providing barriers for carrier diffusion or the production of secondary phases at interfaces. It was not possible to obtain a Mott–Schottky plot for the Ag loaded sample as the Ag had produced a semi-percolating network, which dominated the response.

As $CuWO_4$ is an indirect semiconductor samples of increasing thickness were investigated using UV-Vis spectroscopy to probe optical properties and determine what cross sectional thickness of sample would be required to absorb a significant proportion of the incident irradiation. We show that our samples demonstrate an optical band gap between 2.1 and 2.25 eV, shown in Fig. 5, which is as expected from previous work. We further investigated the impact of cross sectional thickness on the light absorption of the samples and demonstrate that the band gap does not change with cross sectional thickness (as can be inferred in Fig. 5). This indicates that as we produce a thicker sample made up of more layers of sol–gel processing we are not producing any secondary phases within the sample.

We do however see a small variation in band gap and we associate these small changes in band gap with experimental variation. Our observed changes in band gap are not consistent with a change in thickness and are likely to be due to inconsistent scattering of light or other changes to the structure of the sample. Of particular interest is the 900 nm sample which is still not completely absorbing all incident light. This is further evidence that the material is an indirect absorber of light. In essence to absorb a significant proportion of incident light the samples are required to be significantly thicker than the carrier diffusion length and this significantly reduces the photocurrent of the sample.

The PEC response of a 250 and a 900 nm thick sample of pure $CuWO_4$ are shown in Fig. 5. The 900 nm thick sample gave a photocurrent of *ca.* 0.18 mA cm^{-2} at 1.23 V *vs.* NHE. This is approximately 50% of the photocurrent for the 250 nm sample which was recorded at 0.38 mA cm^{-2}. It is also interesting to note that the thicker $CuWO_4$ sample demonstrates a flattening of current at higher applied voltages. This flattening of current is associated with a reduction in available carriers at the surface and relates to the low diffusion length and reduced number of carriers. From Fig. 6 it is clear that low carrier mobility of $CuWO_4$ is influencing surface reactions at higher sample thicknesses due to a lack of available carriers at the interface. This conclusion is further reinforced when reviewing Fig. 4, which shows that more light is being absorbed by thicker $CuWO_4$ giving a higher theoretical photocurrent and yet the photocurrent is lower due to low carrier mobility in our films.

Adding Ag nanowires (0.5% w/w) had no significant effect on the optical band gap as is shown in Fig. 7. The band gap was found to be 2.1 eV and is within the experimental range of optical band gaps for all samples that have been made and tested which include films from 200 to 900 in thickness and with and without Ag nanowires. In order to determine the influence of Ag on PEC response three levels of Ag loading 0.01, 0.02 and 0.5% w/w were investigated for a 750 nm thick sample. The cross section of 750 was chosen after testing a number of samples. The 750 nm thick films gave good light absorption with little improvement in light absorption when the sample was thicker but no significant improvement in current for a thinner sample (due to reduced light absorption), and a gradual reduction in current for thicker samples due to low carrier mobility.

The PEC responses for the Ag loaded samples are shown in Fig. 8. The current density for all Ag loaded samples was significantly higher than plain $CuWO_4$. As a comparison the value for pristine $CuWO_4$ at 750 nm thickness approximated to that of the 900 nm thick film indicating that carrier mobility was significantly retarded even though there was good light harvesting from a film over 500 nm in thickness.

The samples with Ag also show an inverse relationship to Ag loading *i.e.* the photocurrent drops as the amount of Ag increases. The change is most significant at the higher loading of Ag. We believe this is indicative of a reduction in volume of

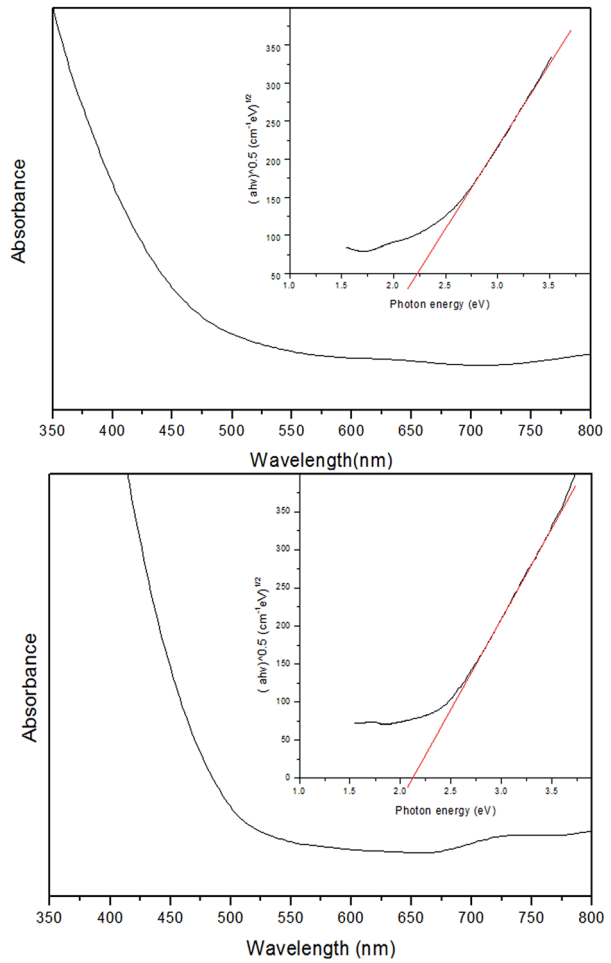

Fig. 5 UV-Vis spectroscopy for a typical 200 nm (top) and 900 nm (bottom) film of $CuWO_4$, with the inset indicating the absorption threshold as determined using the indirect Tauc relationship. The *y*-axis in the case of the major figure is arbitrary absorbance. The absorption onset is shown to range from 2.1 to 2.25 eV. It should be noted that the 900 nm thick film does not show complete light absorption due to the indirect nature of the semiconductor.

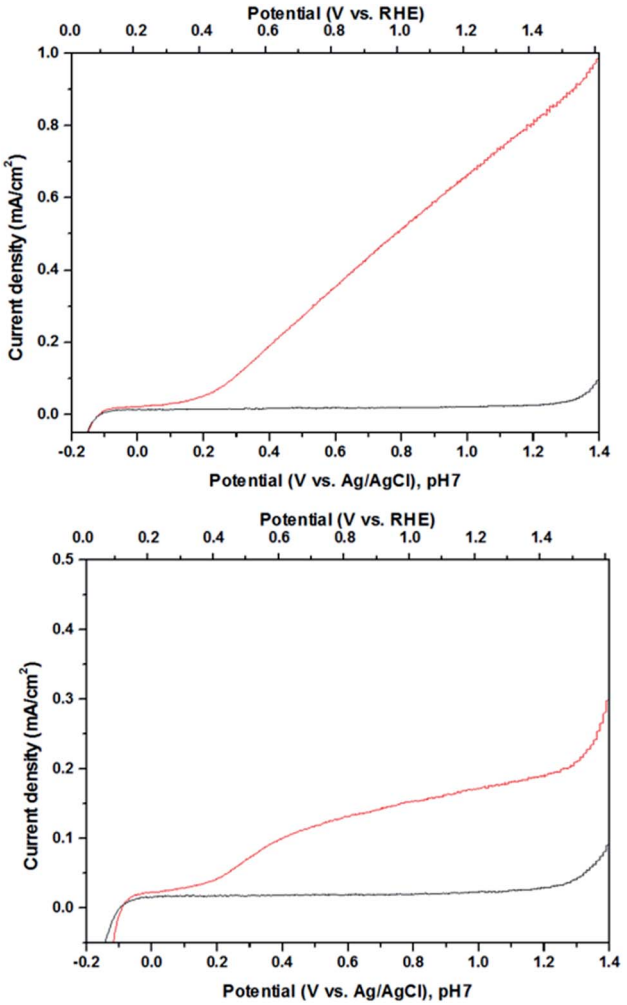

Fig. 6 Linear sweep voltammetry of a $CuWO_4$ electrode 250 nm (top) and 900 nm (bottom) under AM1.5G (red) and dark (black) measured in buffer at pH 7.4. It is apparent that the photocurrent produced by the 900 nm sample is significantly reduced when compared to the 200 nm sample.

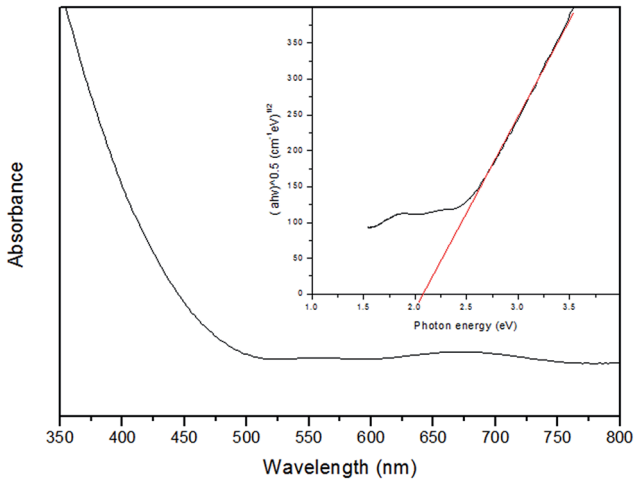

Fig. 7 UV-Vis (main image) and corresponding Tauc analysis (inset) for 250 nm thick $CuWO_4$ with 0.5% w/w Ag nanowire. The *y*-axis in the case of the major figure is arbitrary absorbance. The band gap is found to be around 2.1 eV and is consistent with that expected for this type of material.

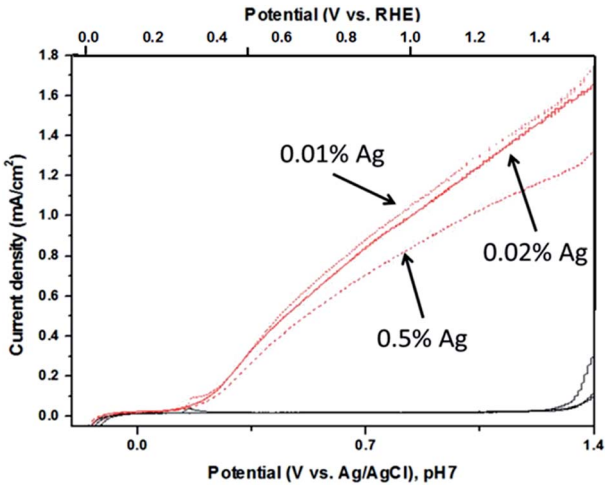

Fig. 8 Linear sweep voltammetry of a 0.5% (dash), 0.02% (solid) and 0.01% (dot) w/w Ag nanowire $CuWO_4$ electrode 750 nm cross section AM1.5G illumination measured in 0.1 M potassium phosphate buffer (pH 7). The baseline of *ca.* 0 mA cm^{-2} represents the current generated in the dark.

photoactive material and internal reflection of light due to the increase in metal nanowires. Although the Ag nanowires are able to increase the current density in our system as the volume of photoactive material reduces the number of photons absorbed and penetration of light into the $CuWO_4$ and so also reduces the photocurrent. What is of most interest is that when Ag nanowires were added the current showed no plateau or saturation at increasing applied bias. This indicates there was no shortage of available carriers at the interface to undergo reaction. The current density with Ag was between 1.0 and 1.5 mA cm^{-2} at 1.23 V *vs.* NHE demonstrating the potential for this material to be used as a photoanode in water splitting.

For pure $CuWO_4$ the point at which the photocurrent switches on was at 0.1 *vs.* NHE. This value is found to be slightly more positive at 0.2 V *vs.* NHE for the Ag nanowire loaded samples. The slight change in flat band potential is likely to be due to surface effects and the introduction of a larger overpotential for the catalytic process.

The photocurrent generated at pH 9 when adjusted for applied bias is approximately 1.5 mA cm^{-2} at 1.23 V *vs.* NHE. This value rivals many other photocatalyst systems when the surface area and surface morphology are taken into account, and is one of the largest reported for similar systems in terms of morphology and structure, Fig. 8. Recent work on nanostructured TiO_2 grown on Si nanowires[37] shows it is possible to generate photocurrents of 1 or 2 mA cm^{-2} under AM1.5G. However, it is more typical to generate photocurrents of less than 1 mA cm^{-2} for TiO_2, considered the bench mark material, under simulated solar light when doped to increase light harvesting. Exceptional results on highly textured and doped TiO_2

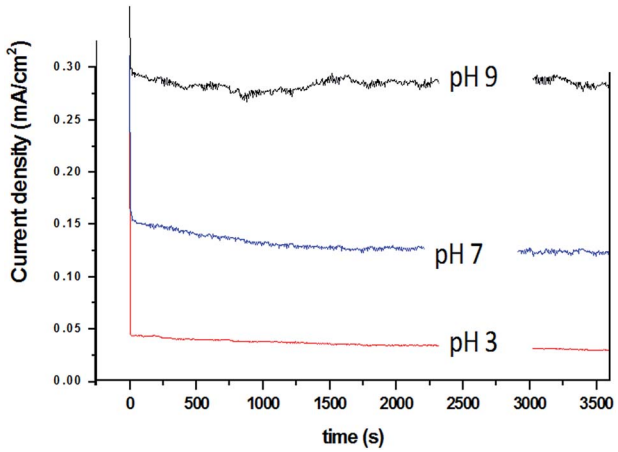

Fig. 9 Stability tests for a 0.5% Ag nanowire $CuWO_4$ electrode 750 nm cross section under AM1.5G illumination measured at pH 9, 7 and 3 using an applied potential of 1.23 V *vs.* NHE. When scaled for applied bias *vs.* NHE at pH 9 the sample is producing *ca.* 1.5 mA cm^{-2} at 1.23 V *vs.* NHE.

have been shown to reach 2 or 3 mA cm^{-2} with associated splitting of water.[38] In the light of the previous results and significant work undertaken on TiO_2 the measured photocurrent of 1.5 mA cm^{-2} for the Ag loaded $CuWO_4$ indicates the promise of this material as an alternative candidate for an efficient photoanode.

The stability of pure $CuWO_4$ has been shown to be good. Using a 750 nm thick sample of 0.5% Ag w/w $CuWO_4$ we have tested the stability of the hybrid catalyst system. Under three pH environments 3, 7 and 9, we show that Ag–$CuWO_4$ was stable with only negligible changes to the photocurrent for 1 hour under AM1.5G illumination, shown in Fig. 9.

The Faradaic efficiency of the system was measured to be 31% using pure water as the fuel source to give the expected 2 : 1 ratio of gaseous products. These values were obtained under AM1.5G and at an applied bias of 1 V *vs.* Ag/AgCl. The rate of evolution of gases in high purity water is shown in Fig. 10.

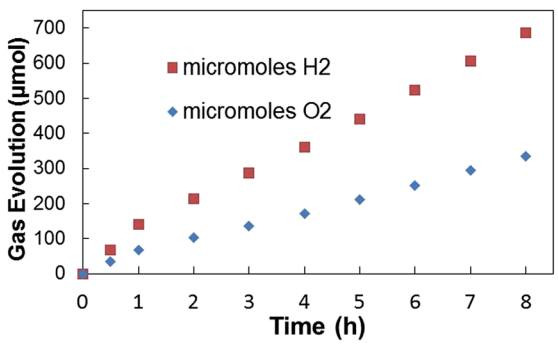

Fig. 10 Evolution of H_2 and O_2 over a 0.01% Ag loaded $CuWO_4$ catalyst in pure water at 1 V *vs.* saturated Ag/AgCl and AM 1.5G illumination with a Pt counter electrode.

Conclusions

We have developed a sol–gel process producing Ag nanowire loaded $CuWO_4$ films that present significantly enhanced photocurrents under AM 1.5G when compared to pristine $CuWO_4$. Our improved photocurrent comes from the ability of the Ag to act as both a catalytic surface and also to enhance carrier mobility within the $CuWO_4$ film. The maximum current density of 1.5 mA cm^{-2} at 1.23 V *vs.* NHE and pH 9 is very competitive against many other semiconductor systems when used as a photoanode. Our measured Faradaic efficiency was 31% indicating that a significant over potential is in effect at the interface.

Acknowledgements

Dr Rory Wilson is thanked for help with X-ray diffraction experiments. Dr Zofi Luklinska is thanked for assistance with scanning electron microscopy.

Notes and references

1 T. Inoue, A. Fujishima, S. Konishi and K. Honda, *Nature*, 1979, **277**, 637–638.
2 L. Li, P. A. Salvador and G. S. Rohrer, *Nanoscale*, 2014, **6**, 24–42.
3 C. X. Kronawitter, L. Vayssieres, S. Shen, L. Guo, D. A. Wheeler, J. Z. Zhang, B. R. Antoun and S. S. Mao, *Energy Environ. Sci.*, 2011, **4**, 3889–3899.
4 Y. Cui, J. Briscoe and S. Dunn, *Chem. Mater.*, 2013, **25**, 4215–4223.
5 M. Ni, M. K. H. Leung, D. Y. C. Leung and K. Sumathy, *Renewable Sustainable Energy Rev.*, 2007, **11**, 401–425.
6 D. W. Zeng, C. S. Xie, B. L. Zhu, R. Jiang, X. Chen, W. L. Song, J. B. Wang and J. Shi, *J. Cryst. Growth*, 2004, **266**, 511–518.
7 S. Chen and L.-W. Wang, *Chem. Mater.*, 2012, **24**, 3659–3666.
8 A. J. Nozik, *Annu. Rev. Phys. Chem.*, 1978, **29**, 189–222.
9 P. M. Jones and S. Dunn, *J. Phys. D: Appl. Phys.*, 2009, **42**, 065408.
10 S. Hoang, S. Guo, N. T. Hahn, A. J. Bard and C. B. Mullins, *Nano Lett.*, 2012, **12**, 26–32.
11 M. Sadeghi, W. Liu, T.-G. Zhang, P. Stavropoulos and B. Levy, *J. Phys. Chem.*, 1996, **100**, 19466–19474.
12 P. R. F. Barnes, D. Blake, J. A. Glasscock, I. C. Plumb, P. F. Vohralik, A. Bendavid and P. J. Martin, in *Solar Hydrogen and Nanotechnology*, ed. L. Vayssieres, SPIE, 2006, vol. 6340, p. 63400P.
13 J. R. Darwent and A. Mills, *J. Chem. Soc., Faraday Trans. 2*, 1982, **78**, 359–367.
14 Q.-H. Zhang, W.-D. Han, Y.-J. Hong and J.-G. Yu, *Catal. Today*, 2009, **148**, 335–340.
15 S. Tokunaga, H. Kato and A. Kudo, *Chem. Mater.*, 2001, **13**, 4624–4628.
16 H. Kato, M. Hori, R. Konta, Y. Shimodaira and A. Kudo, *Chem. Lett.*, 2004, **33**, 1348–1349.
17 J. E. Yourey and B. M. Bartlett, *J. Mater. Chem.*, 2011, **21**, 7651–7660.
18 N. Gaillard, Y. Chang, A. Braun and A. DeAngelis, *MRS Proceedings*, 2012, **1446**, mrss12-1446-u02-08.

19 N. V. Burbure, P. A. Salvador and G. S. Rohrer, *Chem. Mater.*, 2010, **22**, 5831–5837.
20 P. M. Jones, D. E. Gallardo and S. Dunn, *Chem. Mater.*, 2008, **20**, 5901–5906.
21 S. Dunn, *J. Appl. Phys.*, 2003, **94**, 5964–5968.
22 S. Dunn, S. Sharp and S. Burgess, *Nanotechnology*, 2009, **20**, 115604.
23 S. S. Roy, H. Gleeson, C. P. Shaw, R. W. Whatmore, Z. Huang, Q. Zhang and S. Dunn, *Integr. Ferroelectr.*, 2000, **29**(3–4), 189–213.
24 D. Tiwari and S. Dunn, *Mater. Lett.*, 2012, **79**, 18–20.
25 S. Dunn and D. Tiwari, *Appl. Phys. Lett.*, 2008, **93**, 92905.
26 Y. Yun and E. I. Altman, *J. Am. Chem. Soc.*, 2007, **129**, 15684–15689.
27 J. H. Kennedy and K. W. Frese, *J. Electrochem. Soc.*, 1978, **125**, 709–714.
28 C. Santato, M. Odziemkowski, M. Ulmann and J. Augustynski, *J. Am. Chem. Soc.*, 2001, **123**, 10639–10649.
29 J. Y. Zheng, G. Song, C. W. Kim and Y. S. Kang, *Electrochim. Acta*, 2012, **69**, 340–344.
30 M. A. Damián, Y. Rodriguez, J. L. Solis and W. Estrada, *Thin Solid Films*, 2003, **444**, 104–110.
31 M. Denk, D. Kuhness, M. Wagner, S. Surnev, F. R. Negreiros, L. Sementa, G. Barcaro, I. Vobornik, A. Fortunelli and F. P. Netzer, *ACS Nano*, 2014, **8**, 3947–3954.
32 N. Gaillard, Y. Chang, A. DeAngelis, S. Higgins and A. Braun, *Int. J. Hydrogen Energy*, 2013, **38**, 3166–3176.
33 J. A. Seabold and K.-S. Choi, *Chem. Mater.*, 2011, **23**, 1105–1112.
34 J. M. Bolts and M. S. Wrighton, *J. Phys. Chem.*, 1976, **80**, 2641–2645.
35 S. M. Hatch, J. Briscoe, a. Sapelkin, W. P. Gillin, J. B. Gilchrist, M. P. Ryan, S. Heutz and S. Dunn, *J. Appl. Phys.*, 2013, **113**, 204501.
36 S. M. Hatch, A. Sapelkin, G. Cibin, R. Taylor, A. Dent, J. Briscoe and S. Dunn, *J. Appl. Phys.*, 2013, **114**, 153517.
37 J. Shi and X. Wang, *Energy Environ. Sci.*, 2012, **5**, 7918–7922.
38 G. Wang, H. Wang, Y. Ling, Y. Tang, X. Yang, R. C. Fitzmorris, C. Wang, J. Z. Zhang and Y. Li, *Nano Lett.*, 2011, **11**, 3026–3033.